Lasers in Manufacturing Conference 2021

Estimating heat accumulation upon ultrafast laser irradiation

Liliana Cangueiro[a,*], Thomas Kiedrowski[b], Nikolai Schroeder[c], David Bruneel[a], Andrés Fabián Lasagni[c], J. A. Ramos-de-Campos[a]

[a]*Lasea, Rue Louis Plescia, 31, 4102 Seraing, Belgium*
[b]*Robert Bosch GmbH, Robert-Bosch-Campus 1, 71272 Renningen, Germany*
[c]*Institut für Fertigungstechnik Technische Universität Dresden, 01062 Dresden, Germany*

Abstract

Ultrafast lasers micromachining results depend on both the processing parameters and the material properties. The obtained thermal effects are negligible if a good combination of processing parameters is chosen. However, optimizing the processing parameters leading to the required surface quality on a given material can be quite complex and time consuming. Within the framework of the European project LAMpAS, we developed a model to estimate the heat accumulation on a surface as a function of the laser fluence, scanning speed and line pitch. The simulation results were correlated with experimental ones on different materials. The predictions of the model allow evaluating the heat distribution on the surface, as well as optimizing the ultrafast laser micromachining strategy yielding negligible thermal damage.

Keywords: Ultrafast laser ablation; thermal effects; simulation

1. Introduction

It has been thoroughly demonstrated in the past years that ultrafast lasers are excellent tools for ablating and micromachining virtually all types of materials (Sugioka et al., 2014). They allow cutting, milling, etching and texturing surfaces with micrometer precision control and the resulting thermal effects are negligible, provided that an optimal set of processing parameters is used. Depending on the material and its thermal properties, if the processing parameters used are not good, typically by combining high fluences with high

* Corresponding author. Tel.: +32 (0) 4 365 02 43 .
E-mail address: lcangueiro@lasea.com

repetition rates and/or low scanning speeds, often the thermal damage can jeopardize the laser application, due to the accumulation of residual heat in the surface regions remaining after ablation.

Aiming at increasing the throughput of ultrashort laser patterning, a high-power (1.5 kW) ultrashort laser operating at a repetition rates up to 10 MHz will be used for direct laser interference patterning of surfaces at high scanning speeds, within the frame of the European project LAMpAS (www.lampas.eu) . The deposition of energy at such a rate requires a careful management and optimization of the processing parameters to minimize the thermal damage. With this objective, we developed a model to estimate the heat accumulation on a surface as a function of the laser energy deposition parameters and the way the beam moves throughout the surface.

2. Heat accumulation model

The extent of the thermal effects obtained upon laser irradiation will depend on the processing parameters and the thermal properties of the material. The radiation fluence (or the accumulated fluence in case of multi-pulse irradiation) is the laser processing parameter that plays the main role in this process, because it determines the ablation mechanism taking place which, in turn, controls the morphology, composition and properties of the ablation surface. Zhigilei et al., 2009, studied by molecular dynamics the ablation of nickel and analyzed, among other things, the variation of the ablation yields and of the melt depth after ablation with the fluence and the ablation mechanisms. They concluded that the ablation yield for spallation and phase explosion was similar despite the differences of fluence and explained this similarity by the fact that the amount of energy required the decomposition of the solid into a mixture of gas and liquid droplets by phase explosion is larger than the energy required for the ejection of liquid by spallation.

The depth of melting is different for the two mechanisms. In the spallation regime, the surface layer of material heats up and melts in stress confinement conditions. About 50 ps after the laser pulse, the relaxation of the mechanical stresses generated in the surface region leads to the partial ejection of the layer. The depth of the liquid layer after ablation is 20 to 30 nm, 1 to 2 ns after the laser irradiation. When ablation occurs by phase explosion only, the most superficial layer of material is expelled and a significant amount of heat remains in the deeper layers, which is transferred to the bulk by heat conduction. This process is illustrated in Fig. 1. Part of the absorbed pulse energy (E_P) is used for ablation if the pulse energy exceeds the ablation threshold but, in the regions where the absorbed energy was insufficient for ablation to take place, other phase transformations may occur. The depth of material that is thermally affected depends on the deposited thermal energy $E_{thermal}$ and on the thermal properties of the material.

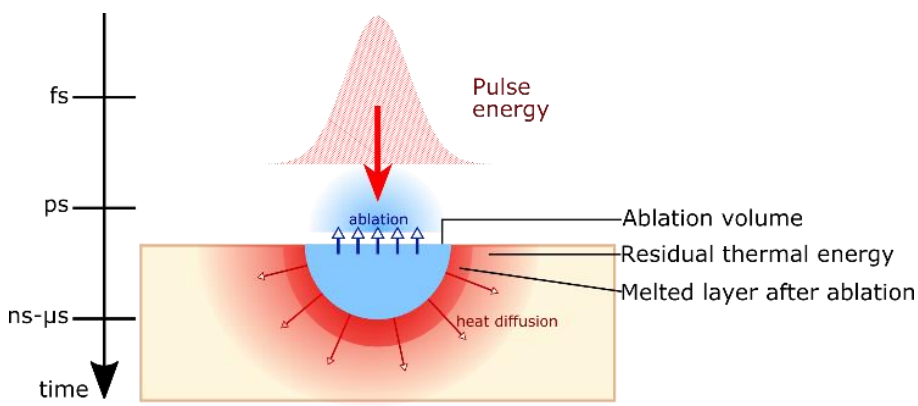

Fig. 1. Illustration of the energy distribution after ultrashort laser irradiation. Adapted from Bauer et al.,2015.

According to Bauer et al., 2015, the temperatures reached by the material after irradiation with a single ultrashort laser pulse with energies leading to ablation can be estimated if we take into account that the heat is concentrated in the most superficial layer of the ablation surface in a time scale shorter than the time required for heat conduction to the bulk. This residual thermal energy can then be considered as an instantaneous superficial point heat source, and the temperature distribution below this surface after a single laser pulse can be calculated by applying the heat conduction equation. For a Gaussian surface heat source, the temperature distribution within an infinite homogeneous solid after a single laser pulse is given by:

$$T_{(x_c,y_c)}^{single\ pulse}(x,y,z,t) = \frac{2E_{thermal}}{\pi\rho c_p\sqrt{\pi\kappa t}(8\kappa t+w_0^2)} exp\left[\frac{(x-x_c)^2+(y-y_c)^2}{4\kappa t}\left(\frac{w_0^2}{8\kappa t+w_0^2}-1\right)\right] exp\left(\frac{-z^2}{4\kappa t}\right) \quad (1)$$

where $(x-x_c)$, $(y-y_c)$ and z describe the distances from the center of the point source (x_c, y_c), w_0 is the spot radius at 1/e² of the maximum intensity, t the time after the energy pulse, c_p the material average heat capacity, ρ the mass density and κ the thermal diffusivity.

For multi-pulse irradiation, the distance between pulses is $t_{p-p} = 1/\mathrm{PRR}$, where PRR is the pulse repetition rate. If the beam is scanned on the surface at a speed v, the spot displacement is $dx = v \times t_{p-p}$ and has to be accounted for adjusting the center coordinates of the gaussian beam. The temperature distribution after N pulses is thus given by:

$$T(x,y,z,t) = \sum_{n=0}^{N} T_{(x_{c_n},y_{c_n})}^{single\ pulse}\left(x,y,z,t+nt_{p-p}\right) \quad (2)$$

This same approach can be used to determine the maximum temperature reached per point on a treated surface produced by hatching parallel laser lines distanced by a certain pitch with a determined speed and repetition rate, as illustrated in Fig. 2. We considered that heat propagates from the surface to the infinitely deep bulk of the solid, equally in all directions (x, y, z). We tested two different scanning strategies, by moving the beam in relation to the sample forward or forward and backward (see black lines in Fig. 2). To these lines, we added the time delays corresponding to the acceleration and deceleration ramp times at the end and beginning of each line, respectively, as illustrated by the red dashed lines in Fig. 3. This is the typical behavior of a beam moved in relation to the specimen both, when a galvo scanner or mechanical stages are used.

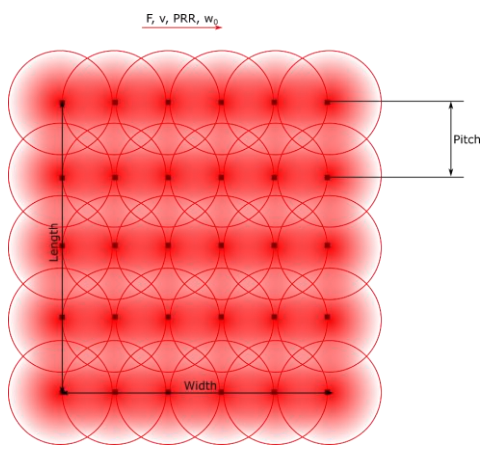

Fig. 2. Disposition of points at which the temperature is determined over an area produced by scanning the beam over parallel lines distanced by a pitch, with a certain fluence, scanning speed and pulse repetition rate.

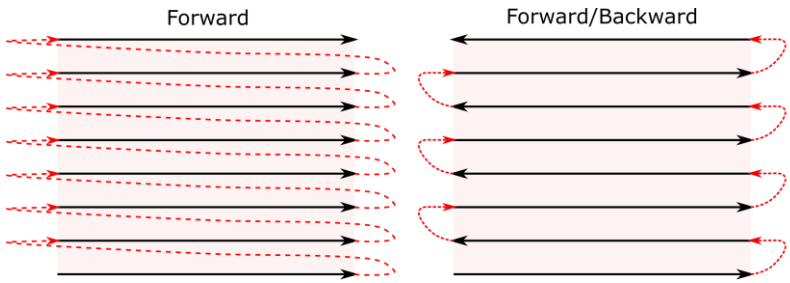

Fig. 3. Scanning strategies simulated.

3. Experimental methods

In order to estimate the amount of residual thermal energy that remained in the material after ablation ($E_{thermal}$ in eq. 1), we ran a calorimetric experiment as described by Bauer et al., ,2015, illustrated in Fig. 4. The laser source used has a pulse width of about 300 fs and 1030 nm central wavelength. The target material was a 1 cm² wide, 500 µm thick foil of stainless steel 316L, which was in close contact with a graphite foil and a thin copper plate which, in turn, had a Pt100 RTD temperature sensor on its back face to measure the temperature upon irradiation. The temperature was monitored upon ablation of hatched squares of 2x2 mm² (30 layers) at 500 kHz repetition rate, 1 m/s beam scanning speed at different peak fluences.

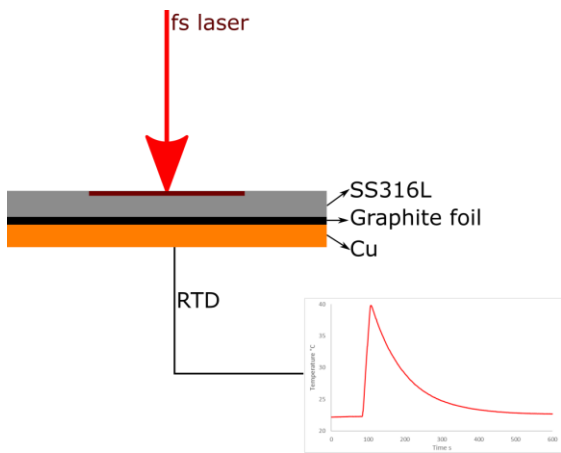

Fig. 4. Schematic illustration of the calorimetric setup used to estimate the residual thermal energy

4. Results and discussion

4.1. Calorimetry

The plot in Fig. 5 shows the evolution of the temperature registered by the RTD sensor on the copper plate back surface during and after irradiation of the stainless steel sample using 8.3 J/cm² peak fluence. From this curve, we extracted (using the method described by Bauer et al., 2015) that the percentage of deposited energy that remained in the material in form of heat was about 28 %, and was about the same also for lower fluences. This is in agreement with other values found in the literature. (Bauer et al., 2015, Gamaly et al., 2002).

This was the value used for the simulations of the temperature distribution and heat accumulation in this work.

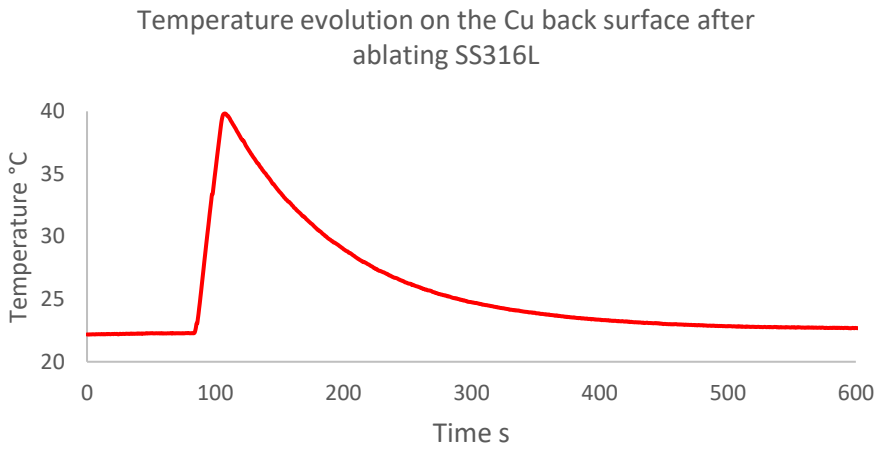

Fig. 5. Temperature evolution monitored on the copper plate back surface during and after irradiation of the stainless steel sample.

4.2. Simulation

The plot in Fig. 6 shows the temperature distributions at different points of a single line scanned at 3 m/s and 1 MHz repetition rate made out of 25 consecutive pulses with 0.5 J/cm² peak fluence. Each of the curves represents the temperature evolution at the spatial coordinates where the first, sixth, eleventh, seventeenth and last pulses hit. According to the literature, the maximum temperature felt at the remaining surface after ablation can be compared to the maximum of the local minima of these plots. These results illustrate that the heat accumulation is not homogeneous all over the irradiated area.

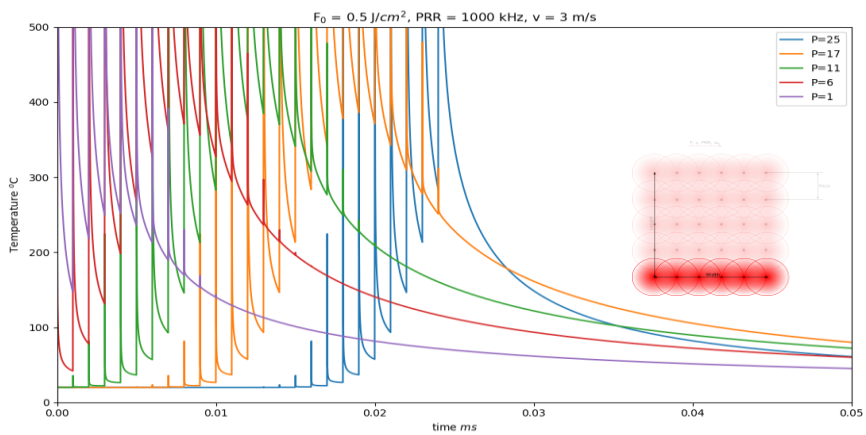

Fig. 6. Temperature evolution at the spatial coordinates where the first, sixth, eleventh, seventeenth and last pulses hit, upon laser scanning a line of 25 consecutive pulses with a scanning speed of 3 m/s, 1 MHz repetition rate and 0.5 J/cm² peak fluence.

The surface plots depicted in Fig. 7 and Fig. 8 illustrate the maximum temperatures per point of surface (corresponding to the maximum of the local minima as shown in Fig. 6) upon laser milling areas 100x100 and 500x500 µm² wide, respectively, using 1 J/cm² peak fluence, 500 kHz repetition rate, 2 m/s scanning speed, 15 µm spot radius and 15 µm of distance between parallel line scans. Heat accumulation was simulated with and without a 200 µs ramp of acceleration plus deceleration delays for the two scanning strategies proposed. The area hatching is done from bottom to top, thus on the positive direction of the Y axis. The pixel resolution of these surface plots is equivalent to the laser pulse to pulse distance. These results show that surface heat accumulation upon ultrashort laser milling highly depends on the size of the treated area for the same set of laser processing parameters. Heat tends to accumulate more towards the end of the milling area, as this zone starts to warm up since the beginning of the area treatment, and so the temperature offset is already high when the beam finally hits this region, thus reaching higher temperatures as compared to the beginning of the treated part, that started out cold. We also observe that not taking into account the time the beam is off to carry out the movement from one line into the next one leads to an overestimation of the maximum temperatures reached, because the material has time to cool down in between hatches. It is in any case virtually impossible to scan an area with times of beam-off negligible enough for thermal diffusivity in metals, so this is an approach that would allow us to estimate the reached temperatures more realistically.

In what concerns to the scanning strategy used, the results demonstrate that it influences the heat distribution on the surface, although this effect is more evident on the 100x100 µm² simulated area, which is likely due to the combined effect of the spatial and temporal distribution of pulses as heat sources. For the larger treated area, the time necessary to scan each line is longer, so the beam takes longer to come back closer to each surface point, giving it time to cool down in the meantime.

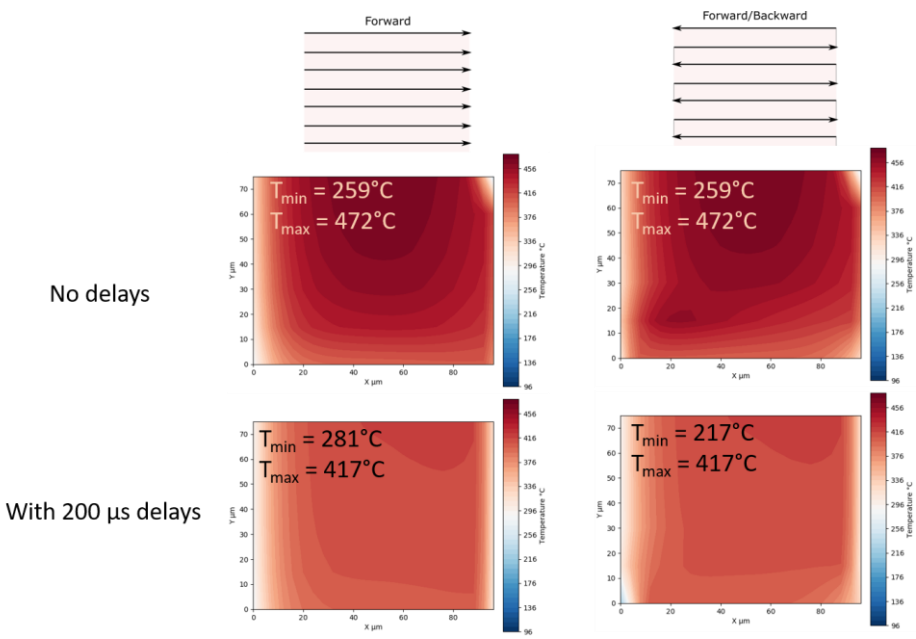

Fig. 7. Surface plots depicting the maximum temperature felt per point of surface upon laser milling of an area 100x100 µm² wide, using 1 J/cm² peak fluence, 500 kHz repetition rate, 2 m/s scanning speed, 15 µm spot radius and 15 µm of distance between parallel line scans, using the two scanning strategies and with and without acceleration and deceleration times. The color bar scale is the same for the four plots.

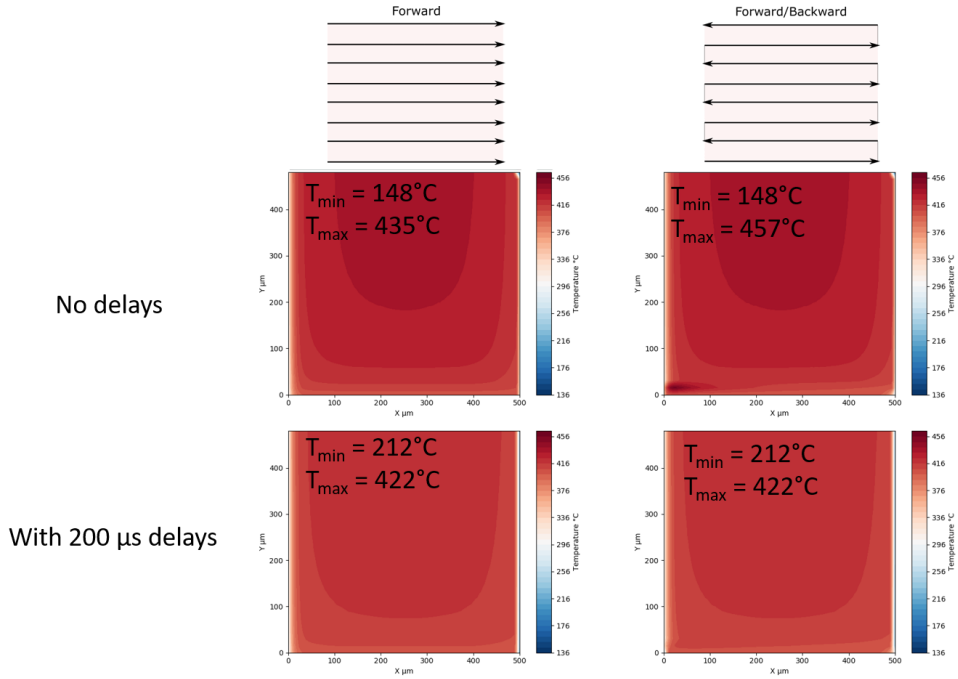

Fig. 8. Surface plots depicting the maximum temperature felt per point of surface upon laser milling of an area 500x500 µm² wide, using 1 J/cm² peak fluence, 500 kHz repetition rate, 2 m/s scanning speed, 15 µm spot radius and 15 µm of distance between parallel line scans, using the two scanning strategies and with and without acceleration and deceleration times. The color bar scale is the same for the four plots.

5. Conclusions

In this work, we simulated the surface heat accumulation on stainless steel upon ultrafast laser milling. Our model allows simulating treated areas using different scanning strategies, and can take into account the acceleration plus deceleration time delays required at the end and beginning of two consecutive hatched lines. The results show that the scanning strategies and the area size influence the general heat distribution and maximum temperatures felt by the surface after ablation, and that the delay times have an important influence on the obtained results. These results may help on choosing the best scanning strategy, areas dimensions and features to minimize the resulting thermal damage while optimizing the cycle time.

Acknowledgements

This project has received funding from the European Union's Horizon 2020 research and innovation programme under grant agreement No 825132. It is an initiative of the Photonics Public Private Partnership (www.photonics21.org). The presented results reflects only the author's view. The EU is not responsible for any use that may be made of the information it contains.

References

Bauer, F., Michalowski, A., Kiedrowski, T., & Nolte, S., 2015. Heat accumulation in ultra-short pulsed scanning laser ablation of metals. Optics Express, 23(2), 1035-1043.

Gamaly, E. G., Rode, A. V., & B., L.-D., 2002. Ablation of solids by femtosecond lasers: Ablation mechanism and ablation thresholds for metals and dielectrics. Physics of Plasmas, 3(9), 949.

Sugioka, K., Cheng, Y., 2014. Ultrafast lasers—reliable tools for advanced materials processing. Light Sci Appl 3, e149.

Zhigilei, L., Lin, Z., & Ivanov, D. S., 2009. Atomistic modeling of short pulse laser ablation of metals: connections between melting, spallation, and phase explosion. The Journal of Physical Chemistry C, 27 113, 11892-11906.